Bulletin of the Seismological Society of America. Vol. 64, No. 1, pp. 45–64. February 1974

GENERALIZED RAY THEORY FOR SHEAR DISLOCATIONS

BY DONALD V. HELMBERGER

ABSTRACT

Generalized ray expansions of the *P*, *SH*, and *SV* displacement potentials resulting from a point-source dislocation are evaluated at the surface of a layered half-space. The Cagniard-de Hoop technique is used to obtain the transient response. The results of this analysis are used to construct synthetic seismograms for a shear dislocation on a vertical fault plane. Comparisons of synthetic and observed seismograms for the Borrego Mountain earthquake (April 9, 1968) at teleseismic distances indicate an equivalent point-source depth of 9 km with the far-field time function approximated by a step function with an exponential decay. This time function fits both the *P* and *S* wave forms. The apparent shift in corner frequency between the *P* and *S* waves for shallow events, as reported by some investigators, is explained by surface reflections.

INTRODUCTION

Recent investigations of the spectra of *P* and *S* waves have demonstrated the practicability of determining earthquake stress drops as well as other important parameters. The technique introduced by Brune (1970) uses the results discussed by Aki (1966) and Keilis-Borok (1960). The basic relationship is that the ratio of fault displacement to fault dimension is proportional to the ratio of stress drop to μ, the rigidity. The proportionality is determined by fault geometry. Applying this result to dislocation theory as well as an intuitive argument on the far-field time history which is

$$s(t) = te^{-\sigma t},$$

where σ is a constant related to the source dimension, allows the corresponding spectrum to be constructed. This hypothetical spectrum is then compared with the spectrum computed from *P* and *S* waves after applying corrections for propagational effects assuming geometrical optics. A partial list of contributors include Wyss (1970), Hanks and Wyss (1972), Wyss and Hanks (1972), Thatcher and Hanks (1973), and Molnar and Wyss (1972). Most of these efforts neglect the effects of earth structure including the interaction with the free surface. These assumptions are probably justified for the case of deep earthquakes but become questionable for shallow events where the phases *pP*, *pS*, *sP*, and *sS* play an important role. Such events are particularly important since fault displacement and dimensions are known independently and allow a test of the method. We will investigate the contributions of these phases in this paper where the generalized ray formalism for a shear dislocation is developed.

Our approach differs from previous spectral studies in that we compute the displacement in the time domain directly from displacement potentials where the various propagational corrections are applied. Synthetic seismograms are then compared directly with observations.

Solutions for various types of point-force configurations have been treated by many authors; some recent contributors are Haskell (1964), Harkrider (1964), Müller (1969), Sato (1969), and Ben-Menahem and Vered (1973). We will limit this paper to point double-couple shear dislocations where generalized ray theory for a layered medium is

discussed. Various useful approximations are given with numerical examples showing the depth effect on the far-field wave forms.

Synthetic P and S waves at teleseismic distances are compared with observations from the Borrego Mountain earthquake, California, April 1968. The far-field time history of

$$s(t) = H(t)e^{-\sigma t},$$

where $H(t)$ is a step function, fits the data considerably better than the time function used by Brune. This time function also becomes dislocation-wise compatible with Brune's near-field expression. In this paper, we have adopted the convention that the near-field time history refers to the time function of the displacement dislocation at the fault whereas the far-field history refers to the derivative of the displacement dislocation. Since Brune's near-field expression starts as a ramp, a compatible far-field expression should start as a step, at least for point sources.

General Solution for Shear Dislocations

Starting with Haskell's representation for shear faulting, it is relatively easy to derive the displacements for double-couple dislocations (see Sato, 1969). We assume an instantaneous motion over a rectangle with dimensions LH. The time history, displacement of one side of the fault relative to the other, is denoted by $D(t)$ with its Fourier transform $\bar{D}(\omega)$. Next, these displacements are expressed in terms of source potentials using cylindrical coordinates with z positive downward. Following Harkrider (1973) and Sato (1969), these expressions become

Strike-slip

$$\begin{aligned}
\bar{\phi}(r, z, \theta, \omega) &= -K \textstyle\int_0^\infty k^2 F_\alpha J_2(kr) \sin 2\theta \, dk \\
\bar{\psi}(r, z, \theta, \omega) &= -K \textstyle\int_0^\infty (\varepsilon v_\beta) F_\beta J_2(kr) \sin 2\theta \, dk \\
\bar{\chi}(r, z, \theta, \omega) &= K k_\beta{}^2 \textstyle\int_0^\infty F_\beta J_2(kr) \cos 2\theta \, dk
\end{aligned} \tag{1}$$

Dip-slip

$$\begin{aligned}
\bar{\phi}(r, z, \theta, \omega) &= -2K \textstyle\int_0^\infty (\varepsilon v_\alpha) k F_\alpha J_1(kr) \sin \theta \, dk \\
\bar{\psi}(r, z, \theta, \omega) &= -K \int_0^\infty \left(\frac{2k^2 - k_\beta{}^2}{k} \right) F_\beta J_1(kr) \sin \theta \, dk \\
\bar{\chi}(r, z, \theta, \omega) &= +K k_\beta{}^2 \int_0^\infty (\varepsilon v_\beta) \frac{F_\beta}{k} J_1(kr) \cos \theta \, dk
\end{aligned} \tag{2}$$

where

$$\begin{aligned}
k_v &= \omega / v_v \\
F_v &= \frac{k \exp(-v_v |z - z_o|)}{v_v} \\
v_v &= (k^2 - k_v{}^2)^{1/2} \\
K &= -\mu \frac{LH \bar{D}(\omega)}{4\pi\rho\omega^2} .
\end{aligned}$$

J_n is the ordinary Bessel function of order n, ω the angular frequency, α and β the compressional and shear velocities, and k the wave number in the horizontal direction (r). We are assuming left lateral motion in the strike-slip case and with the dislocated block moving downward from 0 to 180° in the dip-slip case. The source is located at $z = z_o$ with

$$\varepsilon = \begin{cases} -1 & z < z_o \\ +1 & z > z_o \end{cases}.$$

The vertical, azimuthal, and radial displacements are expressed in terms of these potentials by

$$\begin{aligned} \bar{W}(r, z, \theta, \omega) &= \frac{\partial \bar{\phi}}{\partial z} + \frac{\partial^2 \bar{\psi}}{\partial z^2} + k_\beta{}^2 \bar{\psi} \\ \bar{V}(r, z, \theta, \omega) &= \frac{1}{r}\frac{\partial \bar{\phi}}{\partial \theta} + \frac{1}{r}\frac{\partial^2 \bar{\psi}}{\partial z \partial \theta} - \frac{\partial \bar{\chi}}{\partial r} \\ \bar{Q}(r, z, \theta, \omega) &= \frac{\partial \bar{\phi}}{\partial r} + \frac{\partial^2 \bar{\psi}}{\partial r \partial z} + \frac{1}{r}\frac{\partial \bar{\chi}}{\partial \theta}. \end{aligned} \tag{3}$$

The stress components become

$$\begin{aligned} \bar{P}_{zz} &= 2\beta^2\rho\left[\frac{\partial^2 \bar{\phi}}{\partial z^2} + \frac{\partial^3 \bar{\psi}}{\partial z^3} + k_\beta{}^2 \frac{\partial \bar{\psi}}{\partial z}\right] - \rho(\alpha^2 - 2\beta^2) k_\alpha{}^2 \bar{\phi} \\ \bar{P}_{\theta z} &= \beta^2\rho\left[\frac{2}{r}\frac{\partial^2 \bar{\phi}}{\partial z \partial \theta} + \frac{2}{r}\frac{\partial^3 \bar{\psi}}{\partial z^2 \partial \theta} + \frac{k_\beta{}^2}{r}\frac{\partial \bar{\psi}}{\partial \theta} - \frac{\partial^2 \bar{\chi}}{\partial r \partial z}\right] \\ \bar{P}_{rz} &= \beta^2\rho\left[\frac{2\partial^2 \bar{\phi}}{\partial z \partial r} + \frac{2\partial^3 \bar{\psi}}{\partial z^2 \partial r} + k_\beta{}^2 \frac{\partial \bar{\psi}}{\partial r} + \frac{1}{r}\frac{\partial^2 \bar{\chi}}{\partial z \partial \theta}\right]. \end{aligned} \tag{4}$$

We are primarily concerned with the evaluation of integrals such as expressed in (1) so we need consider only the field variable

$$\bar{\zeta}(r, z, \omega) \equiv -\int_0^\infty F_v J_2(kr)\, dk. \tag{5}$$

Changing variables

$$\omega = -is \quad \text{and} \quad k = -isp$$

we obtain

$$\bar{\zeta}(r, z, s) = \frac{2}{\pi} s \operatorname{Im} \int_0^{i\infty} \frac{p}{\eta_v} K_2(spr) \exp\left(-s\eta_v |z - z_o|\right) dp \tag{6}$$

where

$$\eta_v = \left(\frac{1}{v^2} - p^2\right)^{1/2}$$

and s is the Laplace transform variable and K the modified Bessel function. Equation (6) can be transformed back into the time domain by applying the Cagniard-de Hoop technique (see Gilbert and Helmberger, 1972).

The solution is

$$\zeta(r, z, t) = \frac{2}{\pi}\frac{\partial}{\partial t} \operatorname{Im} \int^t \frac{c(t, \tau)}{(t-\tau)^{1/2}(t-\tau+2pr)^{1/2}} \left(\frac{dp}{d\tau}\right) \frac{p(r)}{\eta_v}\, d\tau, \tag{7}$$

where

$$c(t, \tau(p)) = \cosh\left(2 \cosh^{-1}\left(\frac{t-\tau+pr}{pr}\right)\right)$$

and

$$\begin{aligned} \tau &= pr + \eta_v |z - z_o| \\ \frac{dp}{d\tau} &= \frac{i\eta_v}{(\tau^2 - R^2/V^2)^{1/2}} \end{aligned}$$

where

$$R = (r^2+(z-z_o)^2)^{1/2}.$$

This integral can be evaluated for various values of t after a change of variable (see for example Helmberger, 1968). However, since a relatively large number of integrals needs to be evaluated to describe the motion in a layered medium, we will discuss some useful approximations.

High-frequency motion. Using the asymptotic expansion for the modified Bessel of order n, we have

$$K_n(x) = \left(\frac{\pi}{2x}\right)^{1/2} e^{-x}\left[1+\frac{\mu-1}{8x}+\frac{(\mu-1)(\mu-9)}{2(8x)^2}+\ldots.\right] \tag{8}$$

where $\mu = 4n^2$.

Substituting (8) into (6) and expressing ζ in a series

$$\zeta = \zeta_1+\zeta_2+\zeta_3+\ldots$$

we obtain

$$\begin{aligned}
\zeta_1 &= \frac{2}{\pi}\frac{\partial}{\partial t}\left[\frac{1}{\sqrt{t}} * J_1(t)\right] \\
J_1 &= \mathrm{Im}\left(\frac{\sqrt{p}}{\eta_v}\frac{dp}{dt}\right)\frac{1}{\sqrt{2r}} \\
\zeta_2 &= \left(\frac{15}{8}\right)\frac{2}{\pi}\left[\frac{1}{\sqrt{t}} * J_2(t)\right] \\
J_2 &= \mathrm{Im}\left(\frac{\sqrt{p}}{\eta_v}\frac{dp}{dt}\frac{1}{p}\right)\frac{1}{\sqrt{2r^3}} \\
\zeta_3 &= \frac{105}{128}\left(\frac{2}{\pi}\right)\int dt\left[\frac{1}{\sqrt{t}} * J_3(t)\right] \\
J_3 &= \mathrm{Im}\left(\frac{\sqrt{p}}{\eta_v}\frac{dp}{dt}\frac{1}{p^2}\frac{1}{(2r^5)^{1/2}}\right)
\end{aligned} \tag{9}$$

where the symbol $*$ denotes the convolution operator. This series can be readily evaluated and is applicable for periods such that

$$T < \frac{2\pi r}{3V}.$$

For small distances and long periods, we must use expressions similar to (7).
These expressions can be further approximated by assuming $R/V \gg T$ obtaining

$$\zeta \approx \zeta_1 = \frac{2}{\pi}\frac{\partial}{\partial t}\left[\frac{1}{\sqrt{t}} * \mathrm{Im}\left(\frac{\sqrt{p}}{\eta_v}\frac{dp}{dt}\right)\frac{1}{\sqrt{2r}}\right]. \tag{10}$$

Following the de Hoop transformation, we have

$$t = pr+\eta_v|z-z_o|$$

and

$$\frac{dp}{dt} = \frac{i\eta_v}{(t^2-R^2/V^2)^{1/2}} \qquad t \geqq R/V.$$

If we let $\sin h = r/R$ and $\cos h = (z-z_o)/R$, we obtain

$$p = \frac{\sin h}{R} t + i\left(t^2 - \frac{R^2}{V^2}\right)^{1/2} \frac{\cos h}{R} \tag{11}$$

and

$$\eta_v = \frac{\cos h}{R} t - i\left(t^2 - \frac{R^2}{V^2}\right)^{1/2} \frac{\sin h}{R}. \tag{12}$$

Equation (10) is to be evaluated along the contour defined by (11). A further simplification of (10) can be obtained by making a so-called "first motion" approximation. For values of t near R/V, $p \sim \sin h/V$ and $\eta_v \sim \cos h/V$ and (10) reduces to

$$\zeta(r, z, t) \sim \frac{1}{R} \delta\left(t - \frac{R}{V}\right). \tag{13}$$

In conventional notation, the radiation pattern is expressed in terms of take-off angle $i_h = 180 - h$, where i_h is measured from the vertical. Note that $p = \sin h/V$ (the ordinary ray parameter) in the first-motion approximation. This simplification is useful for comparing Cagniard solutions with standard far-field results.

For the general case of a source embedded in a layered medium, it is convenient to use generalized ray concepts where the generalized reflection and transmission coefficients are expressed in two-dimensional Cartesian coordinates. We define a new potential

$$\bar{\Omega}(r, z, \theta, s) = -(sp)\bar{\psi}. \tag{14}$$

Using expressions (3) and (14), we obtain

$$\begin{aligned}
\bar{W} &= \frac{\partial \bar{\phi}}{\partial z} + sp\, \bar{\Omega} \\
\bar{V} &= \frac{1}{r}\frac{\partial \bar{\phi}}{\partial \theta} - \frac{1}{spr}\frac{\partial^2 \bar{\Omega}}{\partial z \partial \theta} - \frac{\partial \bar{\chi}}{\partial r} \\
\bar{Q} &= \frac{\partial \bar{\phi}}{\partial r} - \frac{1}{sp}\frac{\partial^2 \bar{\Omega}}{\partial r \partial z} + \frac{1}{r}\frac{\partial \bar{\chi}}{\partial \theta}
\end{aligned} \tag{15}$$

and the stress components using (4) and (14) become

$$\begin{aligned}
\bar{P}_{zz} &= 2\beta^2\rho\left(\frac{\partial^2 \bar{\phi}}{\partial z^2} + sp\frac{\partial \bar{\Omega}}{\partial z}\right) + \rho(\alpha^2 - 2\beta^2)\frac{s^2}{\alpha^2}\bar{\phi} \\
\bar{P}_{\theta z} &= \beta^2\rho\left(\frac{2}{r}\frac{\partial^2 \bar{\phi}}{\partial z \partial \theta} - \frac{s^2}{spr}\left(\eta_\beta^2 - p^2\right)\frac{\partial \bar{\Omega}}{\partial \theta} - \frac{\partial^2 \bar{\chi}}{\partial r \partial z}\right) \\
\bar{P}_{rz} &= \beta^2\rho\left(2\frac{\partial^2 \bar{\phi}}{\partial z \partial r} + s^2(\eta_\beta{}^2 - p^2)\bar{\Omega} + \frac{1}{r}\frac{\partial^2 \bar{\chi}}{\partial z \partial \theta}\right).
\end{aligned} \tag{16}$$

We are assuming that these expressions are to be evaluated inside the integrals specified by (6). When $\bar{\chi}$ is independent of r and $\bar{\phi}$ and $\bar{\Omega}$ are independent of θ, these expressions reduce to the form ordinarily used in generalized ray theory. The system specified by (15) and (16) still uncouples into $P-SV$ motion and SH motion as pointed out by Harkrider (1964). This separation allows us to apply the generalized reflection and transmission coefficients used by Helmberger (1968) to handle the effects of layering. We will use this feature in the treatment of the near-field solution discussed in the appendix.

After transforming the potentials from the (ω, k) domain to the appropriate Cagniard domain (s, p), we obtain for the strike-slip case

$$\bar{\phi}(r, z, \theta, s) = -K_o\left(\frac{2}{\pi}\right) \operatorname{Im} \int_o^{i\infty} (p^2) G_\alpha(r, z, p)\, dp \sin 2\theta$$

$$\bar{\Omega}(r, z, \theta, s) = -K_o\left(\frac{2}{\pi}\right) \operatorname{Im} \int_o^{i\infty} (\varepsilon p \eta_\beta) G_\beta(r, z, p)\, dp \sin 2\theta$$

$$\bar{\chi}(r, z, \theta, s) = K_o\left(\frac{2}{\pi}\right) \operatorname{Im} \int_o^{i\infty} \left(\frac{1}{\beta^2}\right) G_\beta(r, z, p)\, dp \cos 2\theta \tag{17}$$

where

$$G_v = \frac{p}{\eta_v} K_2(spr) \exp\left(-s\eta_v |z - z_o|\right).$$

By assuming a step-function time history across the fault, we can express the strength by

$$K_o = \beta_o{}^2 \frac{LHD_o}{4\pi}.$$

The corresponding expressions for the dip-slip case become

$$\bar{\phi}(r, z, \theta, s) = -2K_o\left(\frac{2}{\pi}\right) \operatorname{Im} \int_0^{i\infty} (\varepsilon p \eta_\alpha) H_\alpha \sin\theta\, dp$$

$$\bar{\Omega}(v, z, \theta, s) = K_o\left(\frac{2}{\pi}\right) \operatorname{Im} \int_0^{i\infty} (\eta_\beta{}^2 - p^2) H_\beta \sin\theta\, dp$$

$$\bar{\chi}(v, z, \theta, \mathrm{s}) = K_o\left(\frac{2}{\pi}\right) \operatorname{Im} \int_0^{i\infty} \left(\frac{\varepsilon \eta_\beta}{p\beta^2}\right) H_\beta \cos\theta\, dp \tag{18}$$

where

$$H_v = \frac{p}{\eta_v} K_1(spr) \exp\left[-s\eta_v |z - z_o|\right].$$

The displacements can now be calculated from these expressions by applying the transformations discussed earlier. They can be evaluated exactly by using (7) or approximately by using a series solution similar to (9).

Strike-slip in the far-field. The far-field displacements produced by a double-couple dislocation in a homogeneous medium are well known. We will reproduce these results here by using the first-motion approximations of (17). First we note that from (13) we can write

$$\frac{2}{\pi} \operatorname{Im} \int_0^{i\infty} G_v(r, z, p)\, dp \approx \frac{1}{R} H(t - R/V)$$

so that the potentials (17) for $z > z_o$ become

$$\phi(r, z, \theta, t) = -K_o \frac{\sin^2 h}{\alpha^2} \sin 2\theta \frac{H(t - R/\alpha)}{R}$$

$$\Omega(r, z, \theta, z) = -K_o \frac{\sin h \cos h}{\beta^2} \sin 2\theta \frac{H(t - R/\beta)}{R}$$

$$\chi(r, z, \theta, z) = K_o\left(\frac{1}{\beta^2}\right) \cos 2\theta \frac{H(t - R/\beta)}{R}. \tag{19}$$

The displacements can be calculated directly from these potentials neglecting the $1/R^2$ terms, or they can be computed from expressions (17) and then the integrals approxi-

mated. Letting the index refer to the type of motion produced by ϕ, Ω, and χ, we have for $z > z_o$

$$W_\alpha = K_o \frac{\sin^2 h \cos h}{\alpha^3} \sin 2\theta \frac{\delta(t-R/\alpha)}{R}$$

$$Q_\alpha = K_o \frac{\sin^3 h}{\alpha^3} \sin 2\theta \frac{\delta(t-R/\alpha)}{R}$$

$$W_\beta = -K_o \frac{\sin^2 h \cos h}{\beta^3} \sin 2\theta \frac{\delta(t-R/\beta)}{R}$$

$$Q_\beta = K_o \frac{\sin h \cos^2 h}{\beta^3} \sin 2\theta \frac{\delta(t-R/\beta)}{R}$$

$$V_\beta = K_o \frac{1}{\beta^3} \sin h \cos 2\theta \frac{\delta(t-R/\beta)}{R}. \tag{20}$$

The total displacement produced by these potentials is

$$U_P = (W_\alpha{}^2 + Q_\alpha{}^2)^{1/2} = K_o \frac{\sin^2 h}{\alpha^3} \sin 2\theta \frac{\delta(t-R/\alpha)}{R}$$

$$U_{SV} = (W_\beta{}^2 + Q_\beta{}^2)^{1/2} = K_o \frac{\sin 2h \sin 2\theta}{2\beta^3} \frac{\delta(t-R/\beta)}{R}$$

$$U_{SH} = K_o \frac{1}{\beta^3} \sin h \cos 2\theta \frac{\delta(t-R/\beta)}{R}. \tag{21}$$

Dip-slip in the far-field. The first-motion approximations for (18) can be evaluated following the same procedure. We note that

$$\frac{2}{\pi} \operatorname{Im} \int_0^{i\infty} H_V(r, z, p)\, dp \approx \frac{H(t-R/V)}{R}$$

and the displacement potentials for positive z become

$$\phi(r, z, \theta, t) = -K_o \left(2 \frac{\sin h}{\alpha^2} \cos (h) \right) \sin \theta \frac{H(t-R/\alpha)}{R}$$

$$\Omega(r, z, \theta, t) = K_o \left(\frac{\cos 2h}{\beta^2} \right) \sin \theta \frac{H(t-R/\beta)}{R}$$

$$\chi(r, z, \theta, t) = K_o \left(\frac{\cos h}{\sin h} \frac{1}{\beta^2} \right) \cos \theta \frac{H(t-R/\beta)}{R}. \tag{22}$$

The displacements expressed in component form become

$$W_\alpha(r, z, \theta, t) = K_o \frac{2 \sin h \cos^2 h}{\alpha^3} \sin \theta \frac{\delta(t-R/\alpha)}{R}$$

$$Q_\alpha(r, z, \theta, t) = K_o \frac{2 \sin^2 h \cos h}{\alpha^3} \sin \theta \frac{\delta(t-R/\alpha)}{R}$$

and

$$W_\beta(r, z, \theta, t) = K_o \frac{\sin h \cos 2h}{\beta^3} \sin \theta \frac{\delta(t-R/\beta)}{R}$$

$$Q_\beta(r, z, \theta, t) = K_o \frac{\cos h \cos 2h}{\beta^3} \sin \theta \frac{\delta(t-R/\beta)}{R} \tag{23}$$

and

$$V_\beta = -K_o \frac{\cos h \cos\theta}{\beta^3} \frac{\delta(t-R/\beta)}{R}.$$

The total amplitude of displacement for the P, SV, and SH waves becomes

$$U_P = K_o \frac{\sin 2h \sin\theta}{\alpha^3} \frac{\delta(t-R/\alpha)}{R}$$

$$U_{SV} = K_o \frac{\cos 2h}{\beta^3} \sin\theta \frac{\delta(t-R/\beta)}{R}$$

$$U_{SH} = -K_o \frac{\cos h \cos\theta}{\beta^3} \frac{\delta(t-R/\beta)}{R}. \tag{23}$$

Expressions (21) and (23) are in agreement with those of Knopoff and Gilbert (1959) and Ben-Menahem, Smith, and Teng (1965). The relative polarities of the P and SV waves are indicated in Figure 1. We will use the first-motion approximations discussed

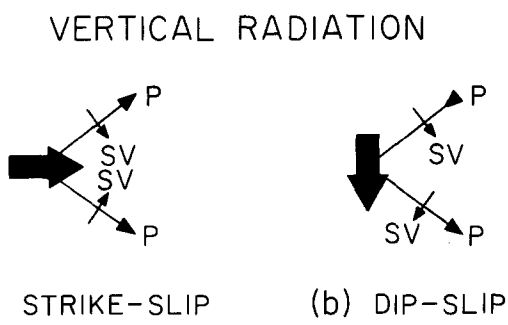

FIG. 1. Polarities of P and SV vertical radiation from a double couple. We are viewing the motion at small positive θ. We have not drawn the block moving to the left in (a) or the block moving up in (b).

in this section to discuss surface interaction for shallow events as viewed at teleseismic ranges, $\Delta > 30°$. At smaller ranges, these approximations are not particularly accurate (see Helmberger, 1973a).

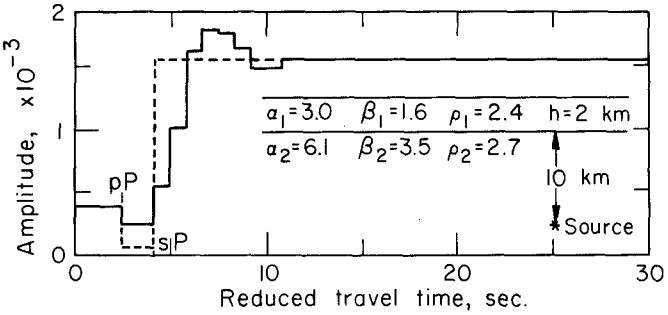

FIG. 2. Effective source radiation from a strike-slip dislocation assuming a step-function time history and a ray parameter = 0.08 sec/km.

RADIATION FROM A SHALLOW DISLOCATION

In this section, we present some results produced from the first-motion approximations of the two types of dislocations discussed earlier. If we limit our applications to teleseismic

distances, we can assume constant ray parameter and evaluate the interaction with the surface by applying time delays for the reflected phases and appropriate amplitude scaling based on source intensity. The result is an effective source function that depends on take-off angle (ray parameter) and azimuth. In the limit of zero depth, our expressions reduce to those of Burridge, Lapwood, and Knopoff (1964).

We first consider a strike-slip event at a depth of 10 km (see Figure 2). Some of the important phases are indicated on the plot. The polarities of P and SV waves leaving the source are indicated in Figure 1. We are assuming a far-field step-time function with the

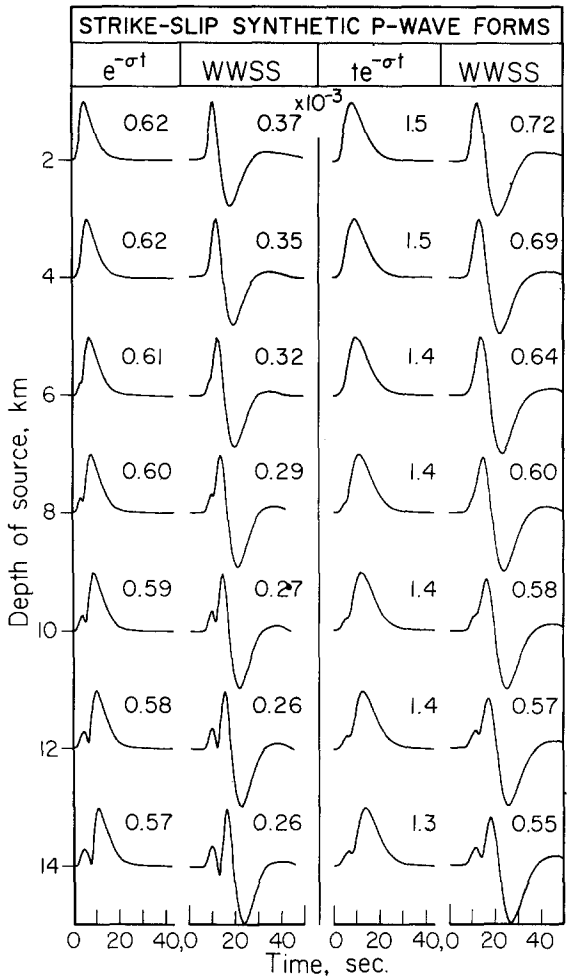

FIG. 3. Variation in the effective synthetic P wave form as a function of source depth.

response starting at the P onset. The dotted curve is the response with the soft surface layer removed whereas the solid curve includes the interaction with the layer. The effect of the soft layer is to limit the domination of the sP phase which is about five times stronger than P for a uniform half-space (see expressions 19). This probably explains why the phase sP is not necessarily overwhelming on short-period recordings. Since the long-period interaction is not particularly influenced by this soft surface layer as indicated in Figure 2, we will omit this thin layer and limit our discussion to the long-period WWSS response computed from the half-space interaction such as the dotted curve in Figure 2.

To obtain the response for an arbitrary far-field time history, we need only to take a derivative and apply a convolution. We also added a source function and Q-operator. We assumed $Q_\alpha/T = 0.5$ and $Q_\beta/T = 0.25$ (see Helmberger, 1973b, for a discussion of the first assumption). We set $Q_\alpha = 2Q_\beta$ from the relationships derived by Anderson *et al.* (1965). The results for two assumed far-field displacement histories are given in Figure 3. For convenience, we will refer to the time history on the left as source I and the Brune type as source II. The column on the left is the displacement before passing through

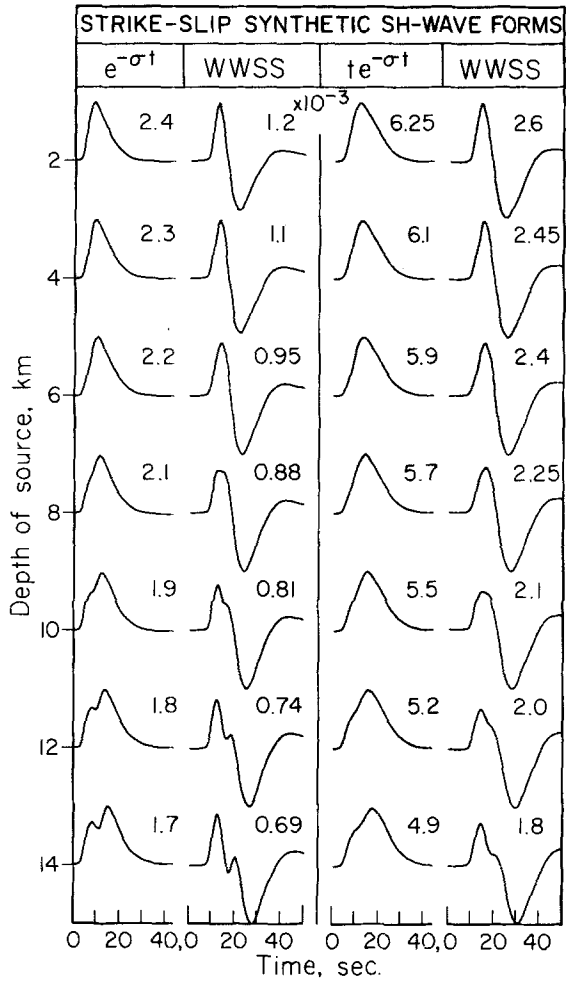

FIG. 4. Variation in the effective synthetic *SH* wave form as a function of source depth.

the instrument. The parameter σ was arbitrarily set at 0.3. The amplitudes are computed assuming $K_0 = 1$ and $R = 1$ for convenience. The amplitude of the synthetic seismogram is appropriate for a magnification of unity. Similar plots are obtained for the *SH* interaction in Figure 4. The effective radiation for the case of dip-slip dislocation is presented in Figures 5 and 6. We chose not to include plots of *SV* since they are very much like *SH* for the assumed ray parameter of 0.05 sec/km.

The domination by the *sP* phase is quite evident in Figures 3 and 5. Changing the depth merely delays the onset of *sP*. In the dip-slip case, the phases *P* and *pP* have the

same polarity whereas, in the strike-slip situation, they have opposite polarity. This feature is apparent in Figures 3 and 5. The strength of sP is considerably stronger in the dip-slip case, as can be seen by comparing (19) with (22). Furthermore, pP and sP are in phase, which explains the large amplitudes in Figure 5 as compared to those of Figure 3. In the dip-slip case, the direct S_H and sS_H have opposite polarity and produce extreme interference at shallow depth. It should be noted that the ground motion actually goes negative for this situation (see Figure 6). The synthetic seismograms reflect this fact as

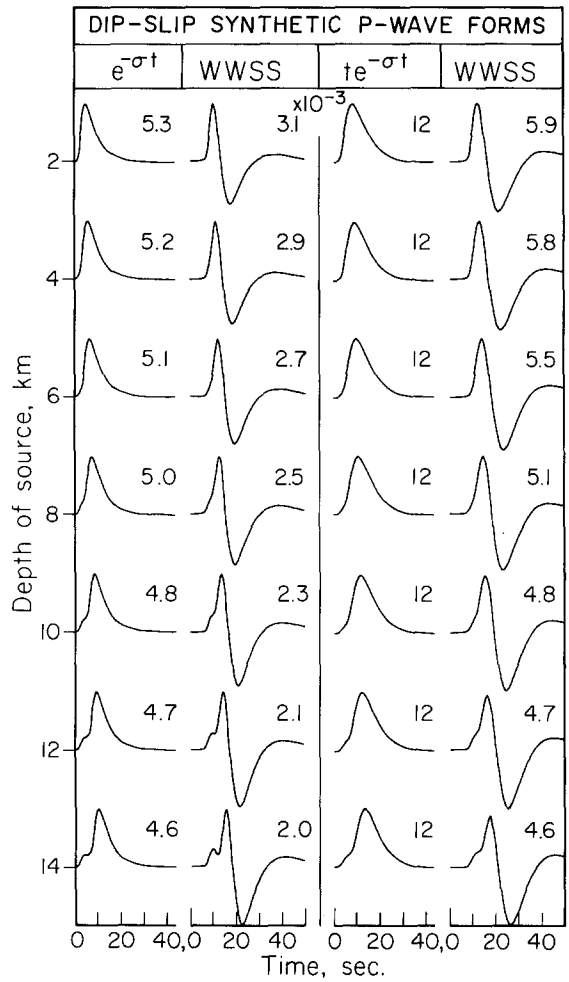

FIG. 5. Variation in the effective synthetic P wave form as a function of source depth.

well by developing an extra peak. The amplitude ratio of SH to P is about a factor of 3 for the strike-slip case whereas, in the dip-slip case, they differ by a factor of two and become strongly depth dependent. The periods of SH and P are comparable in Figures 5 and 6, but they differ considerably in Figures 3 and 4. The reason for the apparent lengthening of SH is that the two phases S and sS have the same polarity. Using more layers, we would expect the interaction to look even more like a ramp function. We think that this is the chief reason for the apparent shift in corner frequency between P and S waves that some observers have noted. We will discuss this feature at length in the next section.

We have not investigated the situation where the ray parameter becomes large enough to produce critical angles. In such situations, the use of first-motion approximations are not particularly useful; that is, the pulses produced by such rays are quite frequency-dependent and must be evaluated using a higher-order approximation such as the first equation of (9).

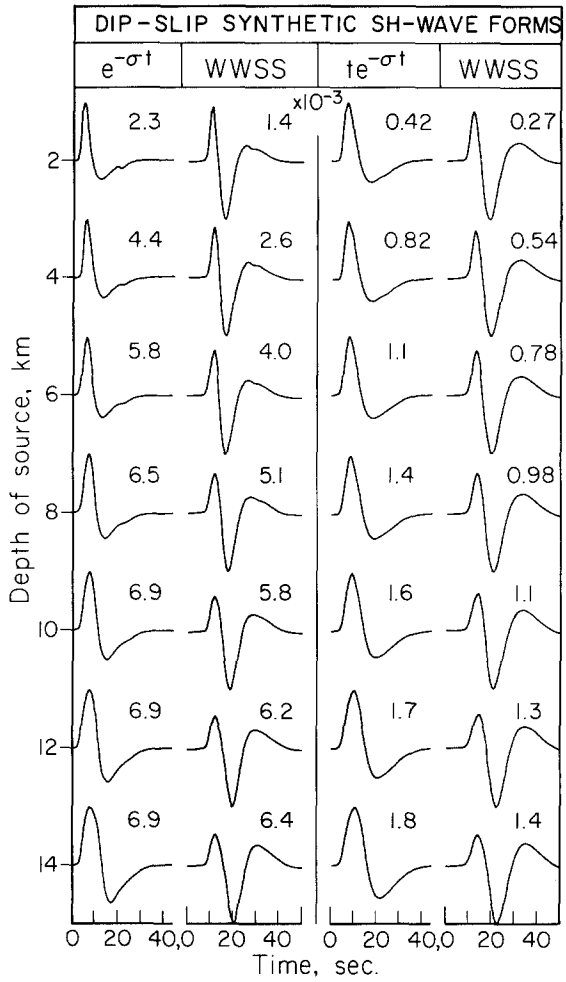

FIG. 6. Variation in the effective synthetic *SH* wave form as a function of source depth.

APPLICATION TO THE BORREGO MOUNTAIN EARTHQUAKE

The interaction of seismic waves with the free surface is obviously a complex phenomenon. This is especially true when the actual faulting reaches the surface. There have been some studies of these complicated problems, for example, Burridge and Halliday (1971). From a practical viewpoint, it seems useful to replace an actual earthquake by an equivalent point source. In general, one would suppose that this equivalent source has a relatively complex radiation pattern, constructed from many finite dislocations interacting with one another, and that the effective time history depends on azimuth and take-off angle. However, there appear to be some relatively simple events occurring on well-developed faults, such as the Borrego Mountain Earthquake which occurred on the

San Jacinto Fault in Southern California in April 9, 1968. This earthquake had a magnitude of 6.4 (Allen *et al.*, 1968) and was predominantly strike-slip. Hanks and Wyss (1972) give a good description of the observed fault dimensions and source parameters as interpreted from Brune's model. The constant σ, chosen to be 0.3 in the previous section, was determined from their analysis.

The event was well recorded on the North American Continent. A sample of the *P*-wave motion is given in Figure 7 as recorded on the short- and long-period components.

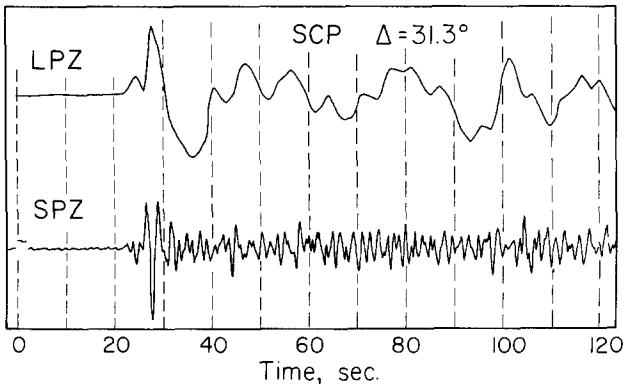

FIG. 7. Recorded motion at the WWSSN station SCP showing the small emergent direct *P* followed by the larger *sP* phase.

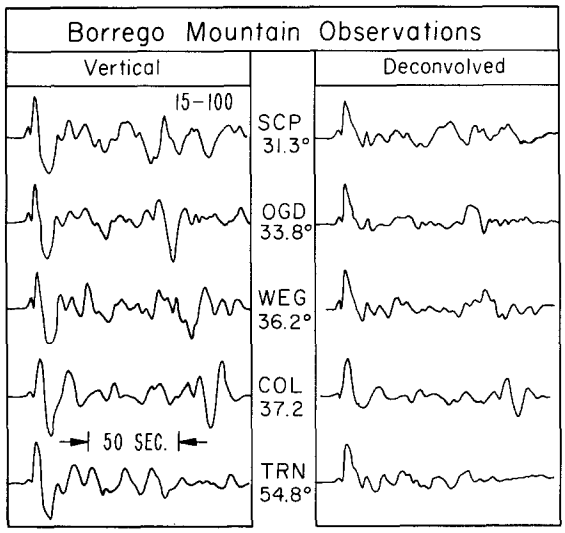

FIG. 8. Observational examples of the *P* wave form from the Borrego Mountain Earthquake and deconvolved vertical ground motion.

The appearance of a relatively large second arrival occurring about 4 sec after the onset is apparent in most of the short-period recordings. It is equally clear on the long-period *P* observations, although it seems small at some azimuths (see Figure 8). A sample of the observed *SH* motion is given in Figure 9 where there is no obvious indication of multi-arrivals. A deconvolution operator was applied to these observed wave forms removing the instrumental response with the results displayed on the right-hand columns of

Figures 8 and 9. We can then compare both the synthetic seismograms and corresponding displacements as discussed in the preceding section with these observations.

After examining Figure 7, it seems reasonable to suppose that the first arrival is the direct P and the large second arrival is the phase sP. Their arrival separation can be used to fix the source depth, although this determination is somewhat model-dependent. Using the model discussed in the previous section, we would predict a depth of 9 km. A comparison with the synthetics for a depth of 10 km is given in Figure 10. Actually, we

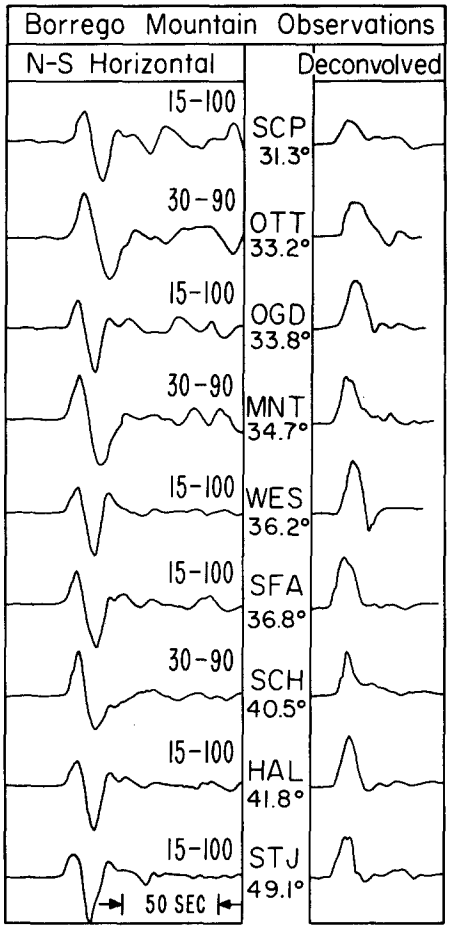

FIG. 9. Observational examples of the S wave forms from the Borrego Mountain Earthquake and associated deconvolved motion.

have used the 10-km depth for the P-wave comparison and the 6-km depth for the SH-wave as given in Figures 3 and 4. This was done as a first-order correction for the difference in ray parameter appropriate for P and S waves. The deconvolved traces for the P waves are rather sharp. For this reason, we used source I in our comparison. The P-wave match is quite good although it could be made better by making the source history more symmetric. The apparent rise time on the deconvolved sP is amazingly short. This suggests a possible directivity effect with the dislocation propagating toward the surface. The comparison between the synthetic and observed SH wave forms is also quite good. It would appear that the observed motion is again more symmetric than the assumed

source. This feature could be produced by adding in a small component of dip-slip (see Figure 6), or it may be caused by a small overshoot. We will not attempt to obtain a better match in this preliminary study because of the large amount of observations that should be used in this type of inversion. Nevertheless, our results indicate a simple mechanism to explain why the apparent corner frequency for S waves is lower than it is for P waves, at least for events that are predominantly strike-slip.

In the above discussion, we compared point-source generated synthetics with data from a finite fault. A correction for the directivity produced by this finiteness can be applied to the synthetics by performing a convolution of our results with a boxcar function. The width of the boxcar will depend on rupture velocity, fault length, and azimuth. Actually, there should be a convolution operator for the vertical finiteness as well. These corrections

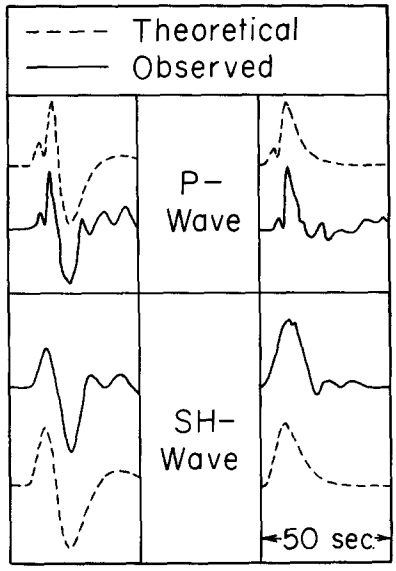

FIG. 10. Comparison of the observed motion at OGD with appropriate synthetics.

will tend to smooth the synthetics considerably and introduce a strong azimuthal effect; that is, the effective far-field time history should be dependent on azimuth. Since the observations do not appear to show these effects, one would suppose that the radiation is coming from a much smaller region than suggested by the surface fault length with a much higher stress drop. A definitive study of both the short- and long-period observations from this event is now in progress to test this hypothesis

CONCLUSIONS

Integral expressions describing the displacement potential for a point-source shear dislocation are discussed. These integrals are reduced to temporal convolutions applying the usual Cagniard-de Hoop technique. The half-space solution in the near-field is developed in a manner that is easily generalized to a layered earth. Various approximate solutions are presented which are especially amenable to numerical evaluation.

First-motion approximations of the exact solutions yield the usual geometrical radiation patterns. These expressions are applied to the problem of effective radiation from a shallow dislocation of the strike-slip and dip-slip type. Synthetic seismograms appropriate

for the long-period WWSS network were generated. Results for the effective P wave, that is, the wave form composed of P, pP, and sP, as plotted versus source depth indicate domination by sP for these two types of orientations. Corresponding results for the effective SH wave show a strong interaction with the surface. For the strike-slip case, these phases add producing an elongated signal. The surface effect tends to shift the corner frequency for S waves to lower values than its P-wave counterpart. The opposite effect is true for the dip-slip situation. Assuming two types of far-field histories, namely $(te^{-\sigma t})$ and $(H(t)e^{-\sigma t})$ where $H(t)$ is the step function, we compared our results with the observations from a strike-slip earthquake, the Borrego Mountain event. The latter source at a depth of 9 km produces the best match. Results from this preliminary study indicate that a large amount of information is embedded in the wave forms of body phases. Detailed analysis of these wave forms at various azimuths and ranges should give us a much clearer picture of source mechanisms than heretofore obtained.

Acknowledgments

I thank Dave Harkrider for his results on potential representations in advance of publication. I am also grateful to Ralph Wiggins for use of his deconvolution program and Gladys Engen who assisted in the numerical analysis.

This research was supported by the Advanced Research Projects Agency of the Department of Defense and was monitored by the Air Force Office of Scientific Research under Contracts F44620-72-C-0078 and F44620-72-C-0083.

Appendix

Generalization to a layered half-space. Using the method of generalized rays, we can construct solutions involving multilayers. The only new feature is the interaction at the free surface in the near-field. We will work out the details for a strike-slip source. The case of the dip-slip or any other orientation can be performed in the same manner.

Starting with expressions (17) we can express the motion at z resulting from a direct and reflected P wave as

$$\bar{\phi}(r, z, \theta, s) = -K_o\left(\frac{2}{\pi}\right) \operatorname{Im} \int_0^{i\infty} (p^2) N_\alpha \frac{p}{\eta_\alpha} K_2(spr) \sin 2\theta \, dp \tag{A1}$$

where

$$N_\alpha = e^{-s\eta_\alpha |z - z_o|} + R_{pp} e^{-s\eta_\alpha (z + z_o)}$$

and the source is situated at z_o.

There will also be a reflected SV wave which can be written

$$\bar{\Omega} = -K_o\left(\frac{2}{\pi}\right) \operatorname{Im} \int_0^{i\infty} (p^2) N_\beta \frac{p}{\eta_\alpha} K_2(spr) \sin 2\theta \, dp \tag{A2}$$

where

$$N_\beta = R_{PS} e^{-s(\eta_\alpha z_o + \eta_\beta z)}.$$

These expressions satisfy the zero stress condition at the free surface as can be seen by substitution into equations (16). The reflection coefficients at a free boundary are those defined by Helmberger (1968) letting one of the solids become a vacuum

$$R_{PP} = \frac{4\beta^4 p^2 \eta_\alpha \eta_\beta - (1-2\beta^2 p^2)^2}{D(p)}$$

$$R_{PS} = \frac{4\beta^2 \eta_\alpha p(1-2\beta^2 p^2)}{D(p)}$$

$$R_{SP} = -\frac{4\beta^2 \eta_\beta p(1-2\beta^2 p^2)}{D(p)}$$

$$R_{SS} = R_{PP}$$

where

$$D(p) = 4\beta^4 p^2 \eta_\alpha \eta_\beta + (1-2\beta^2 p^2)^2.$$

Letting z go to zero or placing the receiver on the surface allows us to write the vertical displacement generated by the direct P wave in simple form

$$\overline{W}_\phi(r, z, \theta, s) = -K_o s\left(\frac{2}{\pi}\right)\int_0^{i\infty} (p^2)\frac{p}{\eta_\alpha} K_2(spr)e^{-s\eta_\alpha z_o} R_{PZ}\, dp \sin 2\theta \tag{A3}$$

where

$$R_{PZ} = \frac{2\eta_\alpha(\eta_\beta{}^2 - p^2)}{\beta^2 R(p)}$$

and

$$R(p) = (\eta_\beta{}^2 - p^2)^2 + 4p^2\eta_\alpha\eta_\beta.$$

R_{PZ} is called the receiver function and describes the interaction of P and SV waves at the surface (see Knopoff *et al.* (1957) for a plane-wave equivalent expression). The motion is up since z is positive downward. Note that for high frequency (see equations 6 and 13)

$$s\frac{2}{\pi}\int_0^{i\infty}\left(\frac{p}{\eta_\alpha}\right)K_2(spr)e^{-s\eta_\alpha z_o}\, dp \sim \frac{\delta(t-R/\alpha)}{R}$$

and (A3) is greater than W_α (20) discussed earlier by a factor of 2 for small $p(z_o \gg r)$. Note that W_ϕ starts as the derivative of the time history and continues to increase as can be seen from the sign of the second term in the power series of expression (9).

The radial displacement produced by the ϕ potential becomes

$$\overline{\phi}_\phi(r, z, \theta, s) = -K_o\left(\frac{2}{\pi}\right)s \operatorname{Im}\int_0^{i\infty} (p^2) M_\alpha e^{-s\eta_\alpha z_o} R_{PR}\, dp \sin 2\theta \tag{A4}$$

where

$$R_{PR} = -\frac{4\eta_\alpha\eta_\beta p}{\beta^2 R(p)}$$

$$M_v = \frac{p}{\eta_v}\left[K_1(spr) + \frac{2}{spr}K_2(spr)\right].$$

The extra complication in M_v is introduced by the radial derivative

$$\frac{\partial}{\partial r}K_2(spr) = -sp\left[K_1(spr) + \frac{2}{spr}K_2(spr)\right]. \tag{A5}$$

The second term in M_v decays $1/r$ faster than the first and has an extra integration. These terms are common in the other displacements and are called near-field terms. Note that $\bar{Q}_\phi$ is basically a longer-period wave than $\bar{W}_\phi$ at small r.

There will also be a tangential component generated by the ϕ potential since (A1) and (A2) contain "θ" dependences.

$$\bar{V}_\phi(r, z, \theta, s) = -K_o\left(\frac{2}{\pi}\right)\frac{1}{r}\,\mathrm{Im}\int_0^{i\infty}(p^2)R_{PT}(2\cos 2\theta)\frac{p}{\eta_\alpha}K_2(spr)\,dp \tag{A6}$$

where

$$R_{PT} = \frac{4\beta^2\eta_\alpha\eta_\beta}{\beta^2 R(p)} = -R_{PR}\left(\frac{\beta^2}{p}\right).$$

This response has the same radiation pattern as the far-field SH, the starting time function of the source, and the Rayleigh-wave shape of Q_ϕ and decays very fast with range. It should be realized that these descriptions can be only observed up to the arrival of $\bar{\Omega}$ and $\bar{\chi}$ or the S waves and that the actual observed surface wave will be a complicated interaction of all three components. However, it is interesting to note that the frequency content of P or its wave shape is dependent on range and on component.

SV-potential. The motion produced by the Ω potential can be evaluated following the same procedure. Performing the indicated algebra, we obtain

$$W_\Omega = K_o\left(\frac{2}{\pi}\right)s\,\mathrm{Im}\int_0^{i\infty}(p\eta_\beta)R_{SZ}\frac{p}{\eta_\beta}K_2(spr)\sin 2\theta\,dp \tag{A7}$$

where

$$R_{SZ} = \frac{4p\eta_\alpha\eta_\beta}{\beta^2 R(p)}.$$

For the radial component, we obtain

$$Q_\Omega = K_o\left(\frac{2}{\pi}\right)s\,\mathrm{Im}\int_0^{i\infty}(p\eta_\beta)R_{SR}M_\beta\sin 2\theta\,dp \tag{A8}$$

where

$$R_{SR} = \frac{2\eta_\beta(\eta_\beta{}^2 - p^2)}{\beta^2 R(p)}.$$

Note that the motion is down and away. There will also be a V component because of the θ dependence given by

$$\bar{V}_\Omega = K_o\left(\frac{2}{\pi}\right)\frac{\mathrm{Im}}{r}\int_0^{i\infty}(p\eta_\beta)R_{ST}(2\cos 2\theta)\frac{p}{\eta_\beta}K_2(spr)\,dp \tag{A9}$$

where

$$R_{ST} = -\frac{2\eta_\beta}{p}\frac{(\eta_\beta{}^2 - p^2)}{\beta^2 R(p)}.$$

The polarity of (A9) is the same as (A6), which means the Rayleigh wave associated with the combination is especially interesting since they will be roughly 45° out of phase at large ranges but in phase at small ranges, where they will have the most influence.

The displacements produced by the $\bar{\chi}$ potential are relatively simple since there is no interaction in the vertical plane. Substituting $\bar{\chi}$ from (18) into (15) we obtain

$$\bar{V}_\chi = -K_o\left(\frac{2}{\pi}\right)s \operatorname{Im}\int_0^{i\infty}\left(\frac{1}{\beta^2}\right)2pM_\beta \cos 2\theta \, dp \,. \tag{A10}$$

A factor of 2 was introduced to describe the free-surface interaction. Equation (A10) contains a near- and far-field term. These responses are in phase with (A6) and (A9) which means there is considerable strength at small ranges. The various expressions of displacement described in this section can be evaluated numerically by applying equation (7) for any value of r or the cheaper version specified by (9). To add layering, one just includes the various generalized transmission and reflection coefficients in the usual manner. Fast evaluation of the first term of expressions given by (9) are discussed by Wiggins and Helmberger (1973).

Similar expressions for a dip-slip dislocation can be obtained by simply replacing the radiation terms enclosed in the brackets at (A3), (A4), (A6), (A7), (A8), and (A9) by the appropriate terms of (18).

References

Allen, C. R., A. Grantz, J. N. Brune, M. M. Clark, R. V. Sharp, T. G. Theodore, E. W. Wolfe, and M. Wyss (1968). The Borrego Mountain, California, earthquake of April 9, 1968: A preliminary report, *Bull. Seism. Soc. Am.* **58,** 1183–1186.

Aki, K. (1966). Generation and propagation of *G* waves from the Niigata earthquake of June 16, 1964, *Bull. Earthquake Res. Inst., Tokyo Univ.* **44,** 73–88.

Anderson, D. L., A. Ben-Menahem, and C. B. Archambeau (1965). Attenuation of seismic energy in the upper mantle, *J. Geophys. Res.* **70,** 1441–1448.

Ben-Menahem, A., S. W. Smith, and T. L. Teng (1965). A procedure for source studies from spectra of long-period seismic waves, *Bull. Seism. Soc. Am.* **55,** 203–255.

Ben-Menahem, A. and M. Vered (1973). Extension and interpretation of the Cagniard–Pekeris method for dislocation sources, *Bull. Seism. Soc. Am.* (in preparation).

Brune, J. N. (1970). Tectonic stress and the spectra of seismic waves from earthquakes, *J. Geophys. Res.* **75,** 4997–5009.

Brune, J. N. (1970). Tectonic stress and the spectra of seismic waves from earthquakes, *J. Geophys. Res.* **75,** 4997–5009.

Burridge, R. and G. S. Halliday (1971). Dynamic shear cracks with friction as models for shallow-focus earthquakes, *Geophys. J.* **25,** 261–283.

Burridge, R., E. R. Lapwood, and L. Knopoff (1964). First motions from seismic sources near a free surface, *Bull. Seism. Soc. Am.* **54,** 1889–1913.

Gilbert, F. J. and D. V. Helmberger (1972). Generalized ray theory for a layered sphere, *Geophys. J.* **27,** 57–80.

Hanks, T. C. and M. Wyss (1972). The use of body-wave spectra in the determination of seismic source parameters, *Bull. Seism. Soc. Am.* **62,** 561–589.

Harkrider, D. G. (1964). Surface waves in multilayered elastic media, I. Rayleigh and Love waves from buried sources in a multilayered elastic half-space, *Bull. Seism. Soc. Am.* **54,** 627–679.

Harkrider, D. G. (1973). Potential representations of a point source dislocation (in preparation).

Haskell, N. A. (1964). Total energy and energy-spectral density of elastic-wave radiation from propagating faults, *Bull. Seism. Soc. Am.* **54,** 1811–1831.

Helmberger, D. V. (1968). The crust-mantle transition in the Bering Sea, *Bull. Seism. Soc. Am.* **58,** 179–214.

Helmberger, D. V. (1973a). Numerical seismograms of long-period body waves, from seventeen to forty degrees, *Bull. Seism. Soc. Am.* **63,** 633–646.

Helmberger, D. V. (1973b). On the structure of the low-velocity zone, *Geophys. J.* (in press).

Keilis-Borok, V. I. (1960). Investigation of the mechanism of earthquakes, *Sov. Res. Geophys.* (English transl.) **4,** 29.

Knopoff, L., R. W. Fredricks, A. F. Gangi, and L. P. Porter (1957). Surface amplitudes of reflected body waves, *Geophysics* **22,** 842–847.

Knopoff, L. and F. Gilbert (1959). Radiation from a strike-slip fault, *Bull. Seism. Soc. Am.* **49,** 163–178.
Molnar, P. and M. Wyss (1972). Moments, source dimensions, and stress drops at shallow-focus earthquakes in the Tonga-Kermadec Arc, *Phys. Earth. Plan. Int.* **6,** 263.
Müller, G. (1969). Theoretical seismograms for some types of point-sources in layered media, *Z. Geophysik* **35,** 347–371.
Sato, R. (1969). Formulations of solutions for earthquake source models and some related problems, *J. Phys. Earth (Tokyo)* **17,** 101–110.
Thatcher, W. and T. C. Hanks (1973). Source parameters of southern California earthquakes (in preparation).
Wyss, M. (1970). Stress estimates of South American shallow and deep earthquakes, *J. Geophys. Res.* **75,** 1529–1544.
Wyss, M. and T. C. Hanks (1972). The source parameters of the San Fernando earthquake inferred from teleseismic body waves, *Bull. Seism. Soc. Am.* **62,** 591–602.

Seismological Laboratory
California Institute of Technology
Pasadena, California 91109
Division of Geological and Planetary Sciences
Contribution No. 2365

Manuscript received July 19, 1973